



Coronin 1C promotes triple-negative breast cancer invasiveness through regulation of MT1-MMP traffic and invadopodia function

Alessia Castagnino, Antonio Castro-Castro, Marie Irondelle, Alan Guichard, Catalina Lodillinsky, Laetitia Fuhrmann, Sophie Vacher, Sonia Agüera-González, Anna Zagryazhskaya-Masson, Maryse Romao, et al.

► To cite this version:

Alessia Castagnino, Antonio Castro-Castro, Marie Irondelle, Alan Guichard, Catalina Lodillinsky, et al.. Coronin 1C promotes triple-negative breast cancer invasiveness through regulation of MT1-MMP traffic and invadopodia function. *Oncogene*, 2018, 37 (50), pp.6425-6441. <10.1038/s41388-018-0422-x>. <hal-02377262>

HAL Id: hal-02377262

<https://hal.science/hal-02377262v1>

Submitted on 23 Nov 2019

HAL is a multi-disciplinary open access archive for the deposit and dissemination of scientific research documents, whether they are published or not. The documents may come from teaching and research institutions in France or abroad, or from public or private research centers.

L'archive ouverte pluridisciplinaire **HAL**, est destinée au dépôt et à la diffusion de documents scientifiques de niveau recherche, publiés ou non, émanant des établissements d'enseignement et de recherche français ou étrangers, des laboratoires publics ou privés.



HAL Authorization

1 Coronin 1C promotes triple-negative breast cancer invasiveness through
2 regulation of MT1-MMP traffic and invadopodia function

3 Alessia Castagnino ¹, Antonio Castro-Castro ¹, Marie Irondelle ^{1,2}, Alan Guichard ¹,
4 Catalina Lodillinsky ^{1,3,4}, Laetitia Fuhrmann ⁵, Sophie Vacher ⁶, Sonia Agüera-
5 González ¹, Anna Zagryazhskaya-Masson ¹, Maryse Romao ⁷, Carole El Kesrouani ⁵,
6 Angelika A. Noegel ⁸, Thierry Dubois ⁹, Graça Raposo ⁷, James E. Bear ¹⁰, Christoph
7 S. Clemen ^{11,8}, Anne Vincent-Salomon ⁵, Ivan Bièche ^{6,12} and Philippe Chavrier ^{1,*}

8 ¹ Institut Curie, PSL Research University, CNRS UMR144, Membrane and
9 Cytoskeleton Dynamics group, 26 rue d'Ulm, F-75005, Paris, France

10 ² Institut Curie, PSL Research University, Cell and Tissue Imaging Facility (PCT-
11 IBiSA), 26 rue d'Ulm, F-75005, Paris, France

12 ³ Universidad de Buenos Aires. Facultad de Medicina. Instituto de Oncología A. H.
13 Roffo. Área de Investigación. San Martín 5481, Buenos Aires C1417DTB, Argentina

14 ⁴ Member of Consejo Nacional de Investigaciones Científicas y Técnicas (CONICET),
15 Argentina

16 ⁵ Institut Curie, PSL Research University, Pathology-Genetics-Immunology
17 Department, 26 rue d'Ulm, F-75005, Paris, France

18 ⁶ Institut Curie, PSL Research University, Pharmacogenomic Unit, Department of
19 Genetics, 26 rue d'Ulm, F-75005, Paris, France

20 ⁷ Institut Curie, PSL Research University, CNRS UMR144, Biogenesis and Functions
21 of Lysosome-Related Organelles group, 26 rue d'Ulm, F-75005, Paris, France

22 ⁸ Center for Biochemistry, Institute of Biochemistry I, Medical Faculty, University of
23 Cologne, Joseph-Stelzmann-Str. 52, 50931 Cologne, Germany

24 ⁹ Institut Curie, PSL Research University, Translational Research Department, Breast
25 Cancer Biology Group, Paris, France

26 ¹⁰ UNC Lineberger Comprehensive Cancer Center and the Department of Cell
27 Biology and Physiology, The University of North Carolina at Chapel Hill, Chapel Hill,
28 NC 27599, USA

29 ¹¹ Department of Neurology, Heimer Institute for Muscle Research, University
30 Hospital Bergmannsheil, Ruhr-University Bochum, Bürkle-de-la-Camp-Platz 1, 44789
31 Bochum, Germany

32 ¹² EA7331, Paris Descartes University, Sorbonne Paris Cité, Faculty of
33 Pharmaceutical and Biological Sciences, 4 avenue de l'observatoire, F-75006, Paris,
34 France

35

36 **Conflict of interest disclosure statement:** Authors have no conflict of interest to
37 declare.

38

39 **Running title:** Coronin 1C regulates breast cancer invasion

40 **Keywords:** Coronin 1C, MT1-MMP traffic, invadopodia, breast cancer, invasion

41 **corresponding author:** Philippe Chavrier, Institut Curie, CNRS UMR144, 26 rue
42 d'Ulm, F-75005, Paris, France. Phone: +33156246359, e-mail:
43 philippe.chavrier@curie.fr

44 **Abstract**

45 Membrane type 1-matrix metalloproteinase (MT1-MMP), a membrane-tethered
46 protease, is key for matrix breakdown during cancer invasion and metastasis.
47 Assembly of branched actin networks by the Arp2/3 complex is required for MT1-
48 MMP traffic and formation of matrix-degradative invadopodia. Contrasting with the
49 well-established role of actin filament branching factor cortactin in invadopodia
50 function during cancer cell invasion, the contribution of coronin-family debranching
51 factors to invadopodia-based matrix remodeling is not known. Here, we investigated
52 the contribution of coronin 1C to the invasive potential of breast cancer cells. We
53 report that expression of coronin 1C is elevated in invasive human breast cancers,
54 correlates positively with MT1-MMP expression in relation with increased metastatic
55 risk and is a new independent prognostic factor in breast cancer. We provide
56 evidence that, akin to cortactin, coronin 1C is required for invadopodia formation and
57 matrix degradation by breast cancer cells lines and for 3D collagen invasion by
58 multicellular spheroids. Using intravital imaging of orthotopic human breast tumor
59 xenografts, we find that coronin 1C accumulates in structures forming in association
60 with collagen fibrils in the tumor microenvironment. Moreover, we establish the role of
61 coronin 1C in the regulation of positioning and trafficking of MT1-MMP-positive
62 endolysosomes. These results identify coronin 1C as a novel player of the multi-
63 faceted mechanism responsible for invadopodia formation, MT1-MMP surface
64 exposure and invasiveness in breast cancer cells.

65 **Introduction**

66 Tumor cell escape and dissemination to distant sites are hallmarks of metastasis, the
67 leading cause of cancer-related death. During breast cancer progression, a key step
68 is the transition from ductal carcinoma in situ (DCIS) - a mass of proliferative cells
69 inside the mammary duct surrounded by an intact myoepithelium and by the
70 basement membrane (BM) - to invasive breast cancers. DCIS-to-invasive breast
71 cancer transition is associated with breakdown of the myoepithelium and the
72 underlying BM and increased metastasis risk. The capacity of cancer cells to remodel
73 extracellular matrix (ECM) barriers is essential for cancer progression and metastasis
74 ¹. Proteolytic remodeling of ECM components by cancer cells mobilizes a group of
75 transmembrane matrix metalloproteinases (MMPs), which includes membrane type 1
76 (MT1)-MMP (aka MMP14) ¹. We recently reported that MT1-MMP is up-regulated in
77 invasive hormone receptor- and epidermal growth factor receptor 2 (HER2)-negative
78 triple-negative breast cancers (TNBCs) as compared to DCIS lesions and normal
79 breast tissue and overexpression predicts the invasive potential of cancerous lesions
80 ².

81 Experimental data based on cancer cell models revealed that ECM remodeling by
82 carcinomatous cells is focused to the pericellular zone ^{3, 4}. Matrix gaps and tunnels
83 forming overtime support infiltrating cell passage through the BM and through the
84 fibrous collagen microenvironment ³. ECM breakdown is mediated by specialized
85 cellular structures of metastatic cells called invadopodia, which form at the plasma
86 membrane in association with ECM fibrils and require actin assembly for their
87 formation ⁵. Invadopodia are the sites of surface exposure and accumulation of MT1-
88 MMP ⁶⁻⁸. Due to difficulties inherent to the submicrometric size and transient nature
89 of invadopodia, fewer studies addressed their formation, dynamics and structure *in*

90 *vivo*. However, recent work based on emerging intravital microscopy techniques,
91 reported the existence of invadopodia-like protrusions in relation with matrix
92 remodeling and metastasis in the natural tumor microenvironment^{9, 10}.

93 Polymerization of invadopodial actin is a multistep process that requires activation of
94 the Arp2/3 complex by nucleation promoting factor (NPF) Wiskott–Aldrich syndrome
95 like protein (N-WASP)¹¹. Regulators of branched actin network dynamics including
96 cortactin (CTTN) and cofilin are likewise essential for invadopodia formation^{6, 12}. The
97 actin-binding protein CTTN promotes actin network assembly by facilitating N-WASP
98 displacement from Arp2/3 complex and stabilizing Arp2/3 complex at branches^{13, 14}.
99 Moreover, CTTN promotes branch stabilization by antagonizing members of the
100 WD40 domain-containing F-actin binding coronin family members, which control
101 debranching and Arp2/3-nucleated filament network disassembly¹⁵⁻¹⁷. Additionally,
102 coronins bind to and inhibit nucleation by the Arp2/3 complex^{15, 18, 19}. All together,
103 these data point to some coordinated functions of CTTN and coronin in the regulation
104 of branched actin network assembly and dynamics.

105 In carcinoma cells, altered phosphorylation and up-regulation of CTTN are
106 associated with increased invadopodia density, promoting invasion and tumor
107 aggressiveness^{12, 20-24}. Similarly, the coronin-family protein coronin 1C (CORO1C
108 aka coronin-3, CRN2) is up-regulated in human cancers including gastric cancers,
109 hepatocellular carcinomas and brain tumors and is correlated with increased
110 invasiveness and metastasis²⁴⁻²⁸. In addition, experimental data have shown that
111 CORO1C is required for degradation of gelatin as a matrix mimic and for formation of
112 invasive protrusions by human glioblastoma cells^{28, 29}.

113 Convergent observations in carcinoma cell lines have identified a pathway involving

late endosome (LE)/lysosome compartments in returning internalized MT1-MMP to invadopodia forming at plasma membrane/ECM contact sites^{7, 8, 23, 30-32}. Docking of MT1-MMP-positive LE/lysosomes to the invadopodial plasma membrane allows surface exposure of the protease possibly through the formation of tubular connections between the limiting membrane of LE/lysosomes and the plasma membrane^{8, 32, 33}. The pathological relevance of this recycling circuitry has been recently established in the context of the invasion program of TNBCs^{23, 31, 32}. A characteristic feature of this mechanism is the presence of F-actin/CTTN-enriched puncta on MT1-MMP-positive LE/lysosomes, which depend on the Arp2/3 complex and its activator WASH complex for their formation^{8, 23, 34, 35}. Perturbation of WASH function affects endolysosomal F-actin/CTTN puncta, interferes with the trafficking of MT1-MMP vesicles to the invadopodial plasma membrane and inhibits MT1-MMP surface exposure and invasion^{8, 32}. Interestingly, a study in macrophages has provided evidence for a role of coronin 1A (CORO1A) in controlling endolysosomal actin assembly in the context of cholesterol trafficking and clearance³⁶. In addition, coordinated functions of CTTN and coronin 1B (CORO1B aka coronin-2) have been implicated in trafficking and plasma membrane docking of multivesicular LEs and regulation of exosome secretion from these compartments in conjunction with the small GTPase Rab27a function^{37, 38}. All together, these data suggest some cooperative functions of CTTN and coronins in the regulation of endolysosomal actin dynamics and trafficking and exocytosis of LE/lysosomal cargo proteins including MT1-MMP.

Here we show that CORO1C is up-regulated in invasive breast cancers and correlates positively with MT1-MMP expression in TNBCs in relation with poor prognosis. Additionally, our results indicate that CORO1C plays a dual function in

139 MT1-MMP-dependent pericellular matrix degradation by regulating invadopodia
140 formation and by controlling the positioning of MT1-MMP storage endolysosomes.

Results

CORO1C is associated with poor outcome in breast cancer. Expression of CORO1A, -B and -C type I coronin family members and pro-invasive MT1-MMP was analyzed by immunoblotting in a panel of 30 breast cancer cell lines. These cell lines were stratified in Normal-like, Luminal, TNBC and HER2⁺ subtypes based on the expression patterns of estrogen and progesterone receptors (ER and PR) and HER2 amplification ³⁹. Expression of hematopoietic-specific CORO1A was detected in Jurkat leukemic T-cells while levels were low to barely detectable in the breast cancer cell lines (Fig. 1AB). In contrast, CORO1B expression was detected in most breast cancer cell lines irrespective of subtypes (Fig. 1A and C). Expression of CORO1C was mostly restricted to TNBC cells similar to MT1-MMP expression pattern (Fig. 1A and DE). Expression of CORO1B and CORO1C mRNAs was analyzed by quantitative RT-PCR in invasive breast cancers using a retrospective cohort of 446 patients with long-term follow-up. It allowed us to examine if variations in CORO1B and -C mRNA expression had a value for patient prognosis (Table S3). We found that 12.1% of breast tumors overexpressed CORO1B mRNA (>3 relative to normal tissues, not shown). Highest CORO1B expression levels were observed in HER2 tumors and positively correlated with Ki-67 proliferation marker (Table S4). However, we did not see an impact of CORO1B expression on the metastasis-free survival (MFS) of breast cancer patients (not shown).

Tumors expressing high levels of CORO1C showed more often ER and PR negativity, correlated with high Ki-67 and epidermal growth factor receptor (EGFR) levels and were more frequently of an advanced grade indicative of an association with bad prognosis (Table S5). Most importantly, CORO1C up-regulation was associated with significantly shorter MFS (Fig. 1F). Multivariate analysis using a Cox

proportional hazard model revealed independent predictive value for MFS of lymph node status, tumor size and grade and CORO1C mRNA expression parameters, indicating that CORO1C expression is a new independent prognostic factor in breast cancer (Table S6, $P=0.0029$).

Based on available RT-qPCR data in the same cohort ², we found a strong positive correlation of CORO1C and MT1-MMP mRNAs (Fig. 1G). Correlation of CORO1C and MT1-MMP expression was similarly observed at the protein level by immunoblotting analysis of a subset of tumor samples selected based on low and high mRNA levels; while there was no obvious correlation with CORO1B or CTTN expression in these tumor samples (Fig. S1AB). Importantly, we analyzed the association of CORO1C and MT1-MMP transcript levels with clinical outcome and found significantly increased metastatic risk in patients with both high MT1-MMP and CORO1C mRNA levels (Fig. 1H). The prognostic significance of 'MT1-MMP and CORO1C expression level' persisted in Cox multivariate regression analysis (Table S7, $P=0.00007$).

Next, we focused our study on CORO1C showing strongest correlation with pro-invasive MT1-MMP and previously implicated in cancer progression and metastasis ^{25, 26, 28}. Changes in CORO1C protein levels in epithelial cancer cells were investigated by immunohistochemistry (IHC) analysis of a tissue microarray (TMA) of invasive breast cancers and adjacent peritumoral tissues from an independent cohort of 136 patients (Table S8). Specificity of CORO1C IHC staining was established by analysis of human MCF10DCIS.com breast cancer-derived cells knocked down for CORO1C expression (Fig. S1C). In peritumoral epithelial tissues, we detected low cytoplasmic levels of CORO1C in luminal cells and strong expression in myoepithelial cells (Fig. 2AB). CORO1C staining was observed in the cytoplasm of

breast carcinoma cells (Fig. 2AB). Quantification and analysis of CORO1C H-score (intensity multiplied by percentage of positively stained cells) revealed significantly higher levels of CORO1C in invasive cancer relative to normal breast tissues (Fig. 2C), in agreement with RNA expression data (Table S5) and protein analysis in breast cancer cell lines (Fig. 1A and D). CORO1C levels were highest in TNBC subtype although difference with other subtypes was not statistically significant (Fig. 2D). Therefore we concluded that CORO1C expression was up-regulated in invasive breast cancers at the mRNA and protein levels, particularly in TNBCs and correlated with worse prognosis and increased metastasis risk in association with MT1-MMP up-regulation. At the mechanistic level, these data suggested some involvement of CORO1C in MT1-MMP-dependent pericellular ECM proteolysis activity during breast tumor progression and dissemination.

CORO1C is required for invadopodia function and tumor cell invasion.

^{GFP}CORO1C was stably overexpressed in MDA-MB-231 cells used as a TNBC model (Fig. S2A). These cells invaded through the 3D fibrous type I collagen network with an elongated morphology typical of this highly invasive mesenchymal cell line (Fig. 3A, low magnification inset and Supplementary Movie S1). CTTN and ^{GFP}CORO1C co-localized in lamellipodia at the edge of invasive protrusions extending within the collagen gel (Fig. 3A, low magnification inset). In addition, arc-shape structures enriched for CTTN and CORO1C were visible in association with collagen fibrils in front of the nucleus, which was located at the rear of the cell (Fig. 3A, inset 1). Strong pericellular collagenolysis was observed in association with the bulbous nuclear cell region as revealed by staining for neoepitope of MMP-cleaved type I collagen (Fig. 3B, yellow). When cells were plated on top of a 2D layer of collagen fibrils, CORO1C was similarly found at the cell edge as well as in curvilinear structures forming in

association with the underlying collagen fibrils, which were positive for the invadopodia protein TKS5 (Fig. 3C)^{8,40}. Collectively, our observations indicated that CORO1C accumulated at proteolytically active invadopodia forming in association with confining collagen fibrils.

The effect of ^{GFP}CORO1C overexpression on the invasive capacity of MDA-MB-231 cells in 3D collagen was assessed. Multicellular spheroids of MDA-MB-231 cells overexpressing GFP or ^{GFP}CORO1C were formed and embedded in the type I collagen gel and invasion was monitored after two days. Overexpression of ^{GFP}CORO1C significantly increased the invasive potential of MDA-MB-231 cells in the 3D collagen gel (Fig. 3DE). CORO1C-dependent invasion required MMP activity as shown by inhibition in the presence of generic GM6001 MMP inhibitor (Fig. 3E). The proinvasive potential of CORO1C was generalized using multicellular spheroids of human MCF10DCIS.com cells overexpressing ^{GFP}CORO1C or YFP as a control (Fig. S3AB).

Actin polymerization is essential for invadopodia formation and function and CORO1C is known to regulate branched actin dynamics. We therefore investigated the contribution of CORO1C to the formation of TKS5-positive invadopodia in MDA-MB-231 cells plated on top of a collagen fibril layer as in Fig. 3C. Overexpression of CORO1C increased significantly the formation of TKS5-positive invadopodia (Fig. 3F). ^{GFP}CORO1C_{R28D/2KE} harboring the R28D, K418E, K419E, K427E, and K428E mutations, which is defective for F-actin binding⁴¹, was diffusely distributed indicating that CORO1C association to invadopodia required binding to F-actin similar to CORO1B and -C recruitment to the lamellipodia^{41,42} (Fig. S3C). Remarkably, actin-binding deficient CORO1C_{R28D/2KE} exerted a dominant inhibitory effect on invadopodia formation (Fig. 3F). An equivalent mutation in CORO1B has been shown

to affect F-actin binding but no other molecular interactions^{15, 42}, which may explain the observed dominant inhibitory potential by titration of important functional partners. In addition, CORO1C was knocked-down by treatment with two independent siRNAs leading to >95% silencing of the protein with no effect on MT1-MMP or TKS5 levels (Fig. S2C). Loss of CORO1C expression reduced by 50-60% the capacity of MDA-MB-231 cells to form TKS5-positive invadopodia in association with the collagen fibrils (Fig. 3G and Fig. S3DE). CORO1B knockdown similarly decreased the formation of TKS5-positive invadopodia by ~50% (Fig. 3G and Fig. S2D). Loss of both CORO1B and -1C did not further reduce invadopodia formation, suggesting that the two isoforms may function together as recently reported¹⁷ (Fig. 3G). Along this line, we found that overexpressed CORO1B^{GFP} accumulated together with MT1-MMP^{mCh} in invadopodia forming in association with collagen fibers (Fig. 3H, inset 1 and Fig. S2B).

Consequences of modulation of CORO1C expression on pericellular matrix degradation in 3D collagen were analyzed by staining of cleaved collagen. Collagen proteolysis mediated by MT1-MMP was strongly up-regulated upon CORO1C overexpression, while ECM degradation was inhibited by CORO1C^{R28D/2KE} or CORO1C silencing (Fig. 3I-K). Collectively, these data indicated that CORO1C had a significant contribution to invadopodia formation and to the invasive program of TNBC cells.

We found that CORO1C co-localized with CTTN at invadopodia (Fig. 3A). Using the same assays, we observed that CTTN knockdown strongly decreased 3D collagen invasion of MDA-MB-231 multicellular spheroids similar to the silencing of MT1-MMP and CORO1C (Fig. S4A-C). In addition, knockdown of CTTN also correlated with a strong reduction of pericellular collagen degradation (Fig. S4DE). Thus we concluded

that up-regulation of CORO1C expression promoted the invasive potential of TNBC by favoring the formation of proteolytically active invadopodia and that CORO1B/1C and CTTN contributed to invadopodia activity suggesting some cooperative function.

CORO1C puncta are observed in association with collagen fibers in breast tumor cells *in vivo*.

Our data identified CORO1C as a key invadopodia component of invasive MDA-MB-231 cells. In agreement with CORO1C requirement during collective invasion by epithelial MCF10DCIS.com breast cancer cells (Fig. S3AB), we also observed a strong association of ^{GFP}CORO1C with TKS5-positive proteolytically active invadopodia forming in association with collagen fibrils in this cell line (Fig. S5A-C). Thus, the distribution of ^{GFP}CORO1C, which localized to invadopodia in breast cancer cells was investigated *in vivo*. We used intravital imaging of mammary MDA-MB-231 and MCF10DCIS.com cell tumor xenografts to visualize ^{GFP}CORO1C in relation with the tumor ECM microenvironment. MDA-MB-231/^{GFP}CORO1C tumor xenografts growing in the mammary gland of SCID mice upon fat pad injection were imaged using 2-photon laser scanning intravital microscopy combined with second harmonic generation (SHG) to visualize collagen fibrils (Fig. 4A). Accumulations of ^{GFP}CORO1C were visible in tumor cells adjacent to collagen fibers (Fig. 4A-C, arrows and insets 1-3). These structures were morphologically heterogeneous ranging from small (submicrometric) puncta (Fig. 4B and insets 1-2) to several μ m-long linear structures similar to curvilinear invadopodia observed in tumor cell lines *in vitro* (Fig. 4C and inset 3). Contrastingly, intravital imaging of fat pad tumors of MDA-MB-231 cells expressing ^{GFP}CORO1C_{R28D/2KE} revealed a diffuse cytosolic distribution of the actin-binding defective CORO1C variant in tumor xenografts (Fig. 4D and inset 4). Therefore, similar to our observations in cultured cells, accumulation of CORO1C in association with collagen fibers *in vivo* required F-actin binding capacity of CORO1C.

The distribution of CORO1C was similarly analyzed during the growth and invasion of MCF10DCIS.com tumor xenograft generated using the intraductal (nipple-) injection model⁴³. We and others reported that injection of this cell line into the duct lumen in SCID mice leads to the formation of DCIS tumor xenografts, which can further progress into invasive lesions upon BM breaching depending on MT1-MMP activity^{2, 43}. Stable overexpression of ^{GFP}CORO1C did not affect MCF10DCIS.com cell's growth in culture (Fig. S5D). Whole-mount and tissue section staining of tumor xenografts analyzed 4-5 weeks after intraductal injection revealed the presence of large epithelial tumors growing within the mammary duct system of SCID mice injected with control or ^{GFP}CORO1C-overexpressing MCF10DCIS.com cells (Fig. S5E, F and H). Tumors presented a necrotic center and some invasive foci of epithelial cells were visible within the mammary gland stroma (Fig. S5E, arrowhead). Tumor burden (foci number and size) was increased in mammary glands injected with ^{GFP}CORO1C-overexpressing cells as compared to control MCF10DCIS.com cells, although differences were not statistically significant 4 to 5-weeks after injection (Fig. S5F-I). These data suggested that ^{GFP}CORO1C-overexpression conferred some growth advantage to MCF10DCIS.com epithelial tumors. Ductal ^{GFP}CORO1C-expressing tumor xenografts were analyzed by intravital 2-photon imaging of GFP and SHG signals. Intraductal tumors were detected as tumor mass surrounded by a thick bed of collagen bundles tangential to the duct (Fig. 4EF). Some microinvasive buds were visible consisting of few ^{GFP}CORO1C-overexpressing epithelial cells that migrated in collective manner within the type I collagen bed (Fig. 4EF and insets 5 and 6). Invasion of ^{GFP}CORO1C cells progressed overtime in the collagen-enriched stroma (compare inset 5 and 6 acquired at 1-week time interval). Intravital imaging at later time point (7-weeks post injection) revealed frankly invasive tumor lesions (Fig.

4G-I). The presence of ^{GFP}CORO1C accumulations forming at the surface of tumor MCF10DCIS.com cells in contact with intratumoral collagen fibers was visible similar to MDA-MB-231 tumors (Fig. 4G-I and inset 7). Collectively, these data indicated that CORO1C accumulated in structures reminiscent of ECM degradative invadopodia, which formed in association with collagen fibrils in the invasive breast tumor xenografts *in vivo*.

Loss of CORO1C causes MT1-MMP-positive LE/lysosome mispositioning and collapse. We have shown that MT1-MMP trafficking to invadopodia depends on actin dynamics on endolysosomes^{8, 23}. The distribution of ^{GFP}CORO1C was analyzed by live cell imaging by confocal microscopy in MDA-MB-231 cells expressing MT1-MMP^{mCh}. As previously described, MT1-MMP^{mCh} accumulated in vesicles that we previously identified as LE/lysosomes^{7, 32}. In addition to ^{GFP}CORO1C localization to lamellipodia, we observed the accumulation of ^{GFP}CORO1C in dynamic and discrete puncta on a majority of MT1-MMP^{mCh}-positive vesicles (Fig. 5A and Supplementary Movie S2). In contrast, F-actin-binding-deficient ^{GFP}CORO1C_{R28D/2KE} was diffuse and cytosolic (Fig. 5B). Endosomal CORO1C-enriched puncta were also positive for CTTN, although a slight shift was visible between the localization of the two proteins in line with the distinct roles played by these proteins in the actin branching cycle^{15, 17} (Fig. 5C, inset). Similarly, CORO1B^{GFP}-positive puncta were visible on MT1-MMP LE/lysosomes (Fig. 3H, inset 2). Cryoimmunoelectron microscopy confirmed the association of ^{GFP}CORO1C-positive puncta on the cytosolic face of LE/lysosomes (Fig. 5D). All together, these data revealed that CORO1C and CORO1B localized to endosomal actin-, CTTN-rich puncta, which depend on WASH and Arp2/3 complexes for their formation and are implicated in MT1-MMP delivery to invadopodia in breast cancer cells^{8, 23, 32, 34, 35}.

We went on analyzing the consequences of CORO1C knockdown on the distribution and morphology of MT1-MMP-positive LE/lysosomes. In control RNAi treated cells, MT1-MMP-positive LE/lysosomes were distributed throughout the cell, with a concentration in the central region of the cell (Fig. 5E and IJ). In cells silenced for CORO1C, MT1-MMP-positive LE/lysosomes were also predominantly localized to the cell center (Fig. 5F and I). In addition, we observed that reduced expression of CORO1C resulted in a tight clustering of MT1-MMP-positive LE/lysosomes in ~70% of the cells (Fig. 5J). We recently identified the scaffolding proteins JIP4 and JIP3 as key players in MT1-MMP endosome positioning by linking LE/lysosomes to the microtubule motors kinesin-1 and dynein/dynactin³². As previously described³², depletion of JIP3 and JIP4 resulted in MT1-MMP endosome dispersion toward the cell periphery (Fig. 5G and IJ and Fig. S6A). Remarkably, triple knockdown of JIP3/JIP4 and CORO1C partially restored some level of scattering of MT1-MMP-positive endosomes (Fig. 5H and IJ). All together, these data suggested that tight clustering of MT1-MMP-positive LE/lysosomes induced upon loss of CORO1C function required retrograde endosomal trafficking in a JIP3/JIP4-dependent manner.

Cells expressing MT1-MMP^{mCh} were fixed and stained for JIP4 and CTTN, and fluorescence signal associated with MT1-MMP^{mCh}-positive compartments was quantified. As previously reported³², JIP4, which is predominantly cytosolic, was detected throughout the cytoplasm and in close proximity to CTTN-positive puncta on the cytosolic face of MT1-MMP endosomes (Fig. 6A and quantification in panels DE, see also Fig. S6C-C'' for lower magnification images). Quantification of fluorescence signal associated with clustered, enlarged MT1-MMP^{mCh}-positive endosomal compartments in CORO1C-depleted cells revealed opposite effects on CTTN and JIP4 association, *i.e.* CTTN association was diminished, while JIP4 accumulated on

MT1-MMP compartments as compared to siNT-treated cells (Fig. 6B and DE and Fig. S6D-E'). Additionally, CTTN knockdown did not alter significantly the association of JIP4 with endosomal membranes (Fig. 6C and DE and Fig. S6B and FF').

We noticed that morphological changes observed in CORO1C-depleted cells including enlargement and perinuclear clustering of LE/Lysosomal compartments were reminiscent of cellular alterations typical of Niemann-Pick disease type C (NPC). Indeed, cholesterol-enriched LEs cluster in the perinuclear area, as a consequence of defective LE/Lysosome traffic and cholesterol clearance in cells of lysosomal storage disease patients including NPC cells ⁴⁴. After fixation, MDA-MB-231 cells treated with control siRNA were stained with the fluorescent cholesterol-binding probe filipin and scattered cholesterol-positive LE structures were observed (Fig. S6G). Treatment of the cells with U18666A, a widely-used amphipathic steroid, which blocks exit of cholesterol from LE/lysosomes and recapitulates the NPC phenotype ⁴⁵, induced tight clustering of cholesterol-laden LE/Lysosomes in the perinuclear cell region (Fig. S6H). Similarly, LE/Lysosome clusters forming in CORO1C-depleted cells were strongly enriched for cholesterol indicative of defective cholesterol exit from the clustered endosomes (Fig. S6IJ).

In order to get further insight at phenotypic alterations of MT1-MMP-positive compartments induced by loss of CORO1C function, MDA-MB-231 cells knocked down for CORO1C were analyzed by transmission electron microscopy. Figure 6F shows the distribution of LE/lysosomes in control cells. CORO1C depletion caused various morphological alterations of LE/lysosomal compartments, which were enlarged, aggregated and fused together and accumulated osmiophilic materials including lamellar inclusions reminiscent of the NPC phenotype (Fig. 6G-I). Collectively, these data indicated that CORO1C played a key role in MT1-MMP

391 LE/lysosome positioning. Loss of CORO1C expression altered the association of
392 JIP4 (and CTTN) on endosomal membranes resulting in LE/lysosome clumps in the
393 perinuclear area possibly responsible for deficient recycling and surface-exposure of
394 MT1-MMP.

Discussion

Previous findings indicated that CORO1C, a member of the coronin family of highly conserved F-actin-binding proteins and regulators of branched actin networks, contributes to invasiveness and metastasis in several cancer types including glioblastoma, primary effusion lymphoma and TNBC^{24, 26-29, 46}. In addition, CORO1C is a biomarker for invasive progression of hepatocellular carcinoma²⁵. However, our understanding of the cellular and molecular mechanisms underlying the role of CORO1C in tumor invasion has remained limited.

Here, we analyzed the expression profile of CORO1C in breast cancer in relation with MT1-MMP, the protease responsible for pericellular matrix degradation by carcinoma cells with major implications in the invasive potential and progression of breast tumors^{2, 47, 48}. In a panel of cell lines representative of the breast cancer molecular subtypes³⁹, CORO1C protein expression was detected mainly in TNBC cells similar to MT1-MMP². CORO1B was broadly expressed irrespective of the molecular subtypes, while expression of hematopoietic-specific CORO1A was low to undetectable¹⁶. Based on RT-qPCR analysis of a retrospective cohort of invasive breast cancers, we found that CORO1C transcript was up-regulated breast cancers and was associated with hormone receptor-negativity, high grade and metastasis risk. In addition, co-up-regulation of CORO1C and MT1-MMP also correlated with significantly higher metastases risk. 'High CORO1C expression' was an independent prognostic factor of breast cancer in multivariate analysis and prognostic significance of 'MT1-MMP and CORO1C expression level' persisted in Cox multivariate regression analysis. Likewise, IHC analysis of invasive breast cancer TMAs confirmed the up-regulation of CORO1C in breast carcinoma at the protein level as compared to normal epithelial tissue. CORO1B mRNA was also up-regulated in a

breast tumor subset, although with no impact on metastasis-free survival. Similar to our findings in breast cancer, published data have correlated CORO1C expression with high-grade gliomas and liver cancers and poor prognosis in stomach cancers^{25, 27, 28}, while no such correlation has been reported between CORO1B and cancer progression. In conclusion, our data, which extend a previous analysis of publicly accessible databases⁴⁶, indicate that CORO1C is up-regulated in hormone receptor-negative breast tumors and associates with poor outcome.

Several studies reported that coronins, including CORO1C, regulate lamellipodial branched actin network and CORO1C activity impinges on cell migration and invasion by cancer cells including MDA-MB-231 TNBC cells in vitro^{28, 29, 46, 49}. Moreover, CORO1C was associated with invasive cell protrusions and has been implicated in the degradation of the matrix mimic gelatin by human U373 glioblastoma-derived cells^{28, 29}. In the present study, we observed that CORO1C co-localized with CTTN and TKS5 in matrix-degradative actin-based invadopodia forming in association with type I collagen fibrils in TNBC cells. Importantly, knockdown of CORO1C inhibited invadopodia formation, pericellular collagenolysis and invasive migration in 3D collagen in two TNBC cell models with distinct mesenchymal (MDA-MB-231) or epithelial (MCF10DCIS.com) features. Thus, our work indicates that CORO1C is required both for single-cell and collective invasion patterns. Association of CORO1B with invadopodia was also observed and CORO1B was required for invadopodia formation. Moreover, loss of both CORO1C and 1B did not further inhibited invadopodia formation, suggesting that both isoforms may function as a complex as previously shown¹⁷.

Actin polymerization is a key component of invadopodia-based invasion program by driving invasive cell protrusions through the matrix and maintaining tight apposition of

surface-exposed MT1-MMP with confining ECM fibrils ^{4, 8}. In addition, binding of MT1-MMP cytosolic tail to the invadopodial actin network is thought to anchor MT1-MMP to these structures ⁵⁰. Assembly of invadopodial actin requires activation of the Arp2/3 complex by N-WASP ^{8, 11, 50}. An antagonism of CTTN and coronin functions has been proposed in the control of a cycle of Arp2/3 branch stabilization and destabilization (^{15-17, 51} and references herein). In addition, coronin and CTTN have been implicated in the regulation of cofilin activity in actin filament turnover, which is crucial during invadopodia assembly ^{11, 51}. We observed that CORO1B/1C and CTTN co-localized at invadopodia. Alike CORO1B/1C, CTTN has been identified as a key regulator of invadopodia formation and its overexpression in various cancer types is associated with tumor progression and metastasis ^{6, 12}. Here, we found that unbalanced CTTN and CORO1B/1C activity upon individual silencing (or inhibition) of either proteins impairs invadopodia formation and function, emphasizing complex and cooperative functions of CTTN and CORO1B/1C in the branching/debranching cycle to replenish Arp2/3 complex and actin pools to promote invadopodia actin dynamics and cancer cell invasion. Overall, our data suggest that CORO1B and CORO1C function together in the mechanism of invadopodia formation and in matrix remodeling. Yet, the reason for the specific association of CORO1C up-regulation - and not CORO1B - with cancer aggressiveness is unclear, we cannot rule out some additional function of CORO1C related to its association with cancer aggressiveness.

Invadopodia's role in matrix degradation has been experimentally established, however the existence and physiological relevance of invadopodia in cancer is questionable because of a lack of direct evidence in vivo. Yet, recent studies provided convincing evidence that invadopodia formation is essential for extravasation and intravasation of tumor cells and promotes lung metastasis in mice

9, 10, 52. Reports based on intravital imaging of tumor cells expressing fluorescently-tagged markers documented the existence of cytoplasmic protrusions identified as invadopodia based on CTTN, N-WASP or TKS5 enrichment and that correlated with cancer cell intra- or extravasation in vivo^{9, 10}. Importantly, intravital imaging of mammary tumor xenografts of GFP-CORO1C-expressing MDA-MB-231 or MCF10DCIS.com cells revealed the presence of GFP-CORO1C accumulations adjacent to collagen fibers in the tumor microenvironment. However, evidence that these structures are proteolytically active is lacking and we cannot formally conclude that GFP-CORO1C accumulations represent *bona fide* invadopodia *in vivo*. Noticeably, GFP-CORO1C-positive structures were observed both in mesenchymal MDA-MB-231 cells and in strands of invasive epithelial MCF10DCIS.com cells supporting the implication of CORO1C in mesenchymal and collective invasion programs.

Branched actin networks also exist on intracellular compartments including endolysosomes where their main function is to sculpt and stabilize endosomal membrane microdomains involved in cargo sorting and recycling^{34, 35, 53}. Endosomal actin patches are nucleated by the Arp2/3-complex upon WASH-mediated activation^{34, 35}. Earlier on, we found that the WASH complex localizes to MT1-MMP-containing LE/lysosomes and its function is required for MT1-MMP trafficking to invadopodia⁸. In addition, several groups reported that depletion of WASH led to enlargement and massive tubulation of the endolysosomal system supporting the idea that WASH-dependent actin assembly may regulate the fission of endosomal recycling tubules^{34, 35, 54}. CTTN was also found to associate with and regulate endosomal actin puncta on MT1-MMP-positive LE/Lysosomes, and it was reported that CTTN loss or deregulation led to the accumulation of enlarged LE/Lysosomes and defective endosomal traffic^{8, 23, 37, 55}. The present study provides corroborating evidence that in

the absence of CORO1C, endolysosomal compartments dramatically enlarged and collapsed in the perinuclear cell area. It has been argued that deficient cargo exit exemplified by massive cholesterol accumulation and organelle obstruction may lead to endosome enlargement⁵⁴. Alteration of the endosomal actin coat may induce endosomal collapse possibly through uncontrolled fusion of individual endosomes. This assumption is supported by findings that interfering with endosomal actin regulatory components such as WASH, CTTN, CORO1A or -C lead to perinuclear redistribution and collapse of endolysosomal compartments^{34-37, 54} (this study).

Moreover, we previously found that the related JIP3 and JIP4 scaffolding proteins regulate the recruitment of minus-end and plus-end microtubule motor complexes to WASH-positive domains³². Loss of JIP3 and JIP4 proteins led to the accumulation of MT1-MMP compartments at the cell periphery indicating unbalanced minus/plus-end motor activities (at minus-end dynein expense)³². Here we found that loss of CORO1C moderately increases JIP3/JIP4 recruitment on MT1-MMP-positive endosomes although the underlying mechanism remains unknown. Interestingly, enhanced recruitment of JIP4 to endolysosomal compartments was recently shown to induce endolysosome collapse into the cell center⁵⁶. Excess JIP3/JIP4 on MT1-MMP endosomes is expected to promote their perinuclear accumulation due to increased dynein activity, possibly favoring endosome collision and collapse. In agreement with this assumption, we found that formation of endosomal clusters upon loss of CORO1C was abrogated when JIP3/JIP4 were silenced. Also to be considered, coordinated functions of coronins and CTTN were also implicated in the regulation of endolysosome docking with the plasma membrane and exocytosis^{37, 38}. All together, our work highlights a molecular framework based on interplay of WASH, CTTN,

519 CORO1C and JIP3/JIP4 function in the regulation of endosome positioning and
520 dynamics as an essential component of MT1-MMP-based metastatic program.

Materials and Methods

Cell culture. MDA-MB-231 cells (ATCC HTB-26) were grown in L15 medium supplemented with 15% fetal calf serum and 2 mM glutamine at 37°C in 1% CO₂. MCF10DCIS.com cell line was purchased from Asterand and maintained in DMEM-F12 medium with 5% horse serum. MDA-MB-231 and MCF10DCIS.com cell lines were checked monthly for mycoplasma contamination using a real-time PCR method (MYCOPLASMACHECK, GATC Biotech AG).

Stable and transient transfection and siRNA treatment. MDA-MB-231 cells stably expressing MT1-MMP^{mCh} have been previously described⁵⁷. Lentiviral constructs encoding GFP-CORO1C or GFP-CORO1C_{R28D/2KE}⁴¹ cloned in pLKO.1 vector have been described²⁹. MDA-MB-231 cells expressing GFP-CORO1C, GFP-CORO1C_{R28D/2KE}, GFP-CORO1C/MT1-MMP^{mCh}, GFP-CORO1C_{R28D/2KE}/MT1-MMP^{mCh} and MCF10DCIS.com cells stably expressing GFP-CORO1C were generated by lentiviral transduction as described⁵⁸. pLL7.0-m1B-EGFP construct encoding CORO1B^{GFP} was provided by J.E. Bear. For transient expression, MDA-MB-231 cells were transfected with plasmid constructs using AMAXA nucleofection (Lonza). Cells were analyzed by live cell imaging 24-48 hr after transfection. For knockdown, MDA-MB-231 cells were treated with the indicated siRNA (50 nM, see Table S1) using Lullaby (OZ Biosciences) and analyzed 72 hours after treatment.

Antibodies and reagents. Antibodies used for this study are listed in Table S2. GM6001 (Millipore) was diluted in ethanol and used at a concentration of 40 µM. Filipin III (stock in DMSO, 0.1 mg/ml µM working concentration) and U18666A (stock in H₂O, 10 µM working concentration) were purchased from Sigma.

Indirect immunofluorescence microscopy. Samples were fixed with 4% paraformaldehyde, permeabilized with 0.1% Triton X-100, and then incubated with specific antibodies (see Table S2). For quantification of CTTN or JIP4 on MT1-MMP^{mCh}-containing endosomes, cells were stained with specific antibodies and z-dimension series of images (z-stacks) were acquired with 0.2 μ m interval with a wide-field Eclipse 90i Upright Microscope (Nikon) by mean of a piezoelectric motor (Physik Instrument), a 100x Plan Apo VC 1.4 oil immersion objective and a cooled interlined charge-coupled device (CCD) camera (CoolSnap HQ2, Roper Scientific). Images were deconvolved⁵⁹, and detection of CTTN or JIP4 on MT1-MMP^{mCh}-containing endosomes from the median plane of the z-stack was performed using a CellProfiler pipeline as previously described^{23, 60}. Briefly, MT1-MMP^{mCh}-containing endosomes were identified by thresholding and intensity-based watershed; CTTN or JIP4 spots in a 3-pixel wide neighborhood around each MT1-MMP^{mCh}-positive vesicle were identified using a Laplacian of Gaussian filter followed by a watershed on the automatically thresholded image. Finally, the total area of CTTN or JIP4 spots was normalized over the total of MT1-MMP^{mCh}-positive vesicles.

Live cell spinning disk confocal microscopy. For live cell confocal spinning disk microscopy, MDA-MB-231 cells stably expressing ^{GFP}Coro1C and MT1-MMP^{mCh} or ^{GFP}CORO1C_{R28D/2KE} and MT1-MMP^{mCh} were plated on glass-bottom dishes (MatTek Corporation) coated with cross-linked gelatin and kept in a humidified atmosphere at 37°C in 1% CO₂. Time-series were acquired using a spinning disk microscope (Roper Scientific) based on a CSU X1 head (Yokogawa) mounted on the lateral port of an inverted microscope (TE-2000U-Nikon) steered by MetaMorph software and equipped with a 60x 1.45 NA oil-immersion objective, a Piezzo Z stage (Mat-City-

Lab), a dual output laser launch that included 491- and 561-nm 50-mW DPSS lasers (Roper Scientific) and a CCD camera (CoolSNAP HQ2).

Analysis of endosome distribution and clustering. For the analysis of the distribution of MT1-MMP^{mCh}-positive endosomes, a MATLAB software has been developed to determine the relative position of each endosome to the cell centroid as previously described ⁶¹.

Invadopodia formation assay. Coverslips were layered with 100 µl of a 2.2 mg/ml solution of acid-extracted type I rat tail collagen (Corning) mixed with AlexaFluor 647-conjugated type I collagen (5% final). After gelling for 3 min at 37°C, the collagen layer was washed gently in PBS and 1 ml of cell suspension (10⁵ cells/ml) was added. Cells were incubated for 90 min at 37°C in 1% CO₂ incubator, then pre-extracted with 0.5% Triton X-100 in 4% paraformaldehyde in PBS during 90 s and fixed in 4% paraformaldehyde in PBS for 20 min. Cells were analyzed by immunofluorescence staining with TKS5 and CTTN antibodies (Table S2), and z-stacks of images were acquired as described above. For quantification of TKS5 associated with curvilinear invadopodia, 5 consecutive planes corresponding to the plasma membrane in contact with collagen fibers were projected and surface covered by TKS5 signal was determined using the thresholding command of ImageJ excluding regions <8 pixels (*i.e.* <1 µm) to avoid non-invadopodial structures. Surface covered by TKS5 was normalized to the total cell surface and values normalized to control cells.

Quantification of pericellular collagenolysis. Cells were trypsinized and resuspended in 0.2 ml of 2.2 mg/ml ice-cold collagen I solution in 1x MEM, pH 7.5 buffer (2.5 x 10⁵ cells/ml). A 40 µl-drop of the cell suspension in collagen was added

on a 18-mm diameter glass coverslip and collagen polymerization was induced by incubation at 37°C for 30 min. Complete medium was added, and the collagen-embedded cells were incubated for 12 hrs at 37°C. Samples were fixed in 4% paraformaldehyde in PBS at 37°C for 30 min, and incubated with Col1-^{3/4}C antibody (2.5 µg/ml) for 2 hrs at 4°C, washed extensively with PBS and counterstained with Cy3-conjugated anti-rabbit IgG antibodies and with DAPI. Image acquisition was performed with an A1R Nikon confocal microscope with a 40× NA 1.3 oil objective using high-sensitivity GaASP PMT detector and a 595 ± 50 nm band-pass filter for red fluorescence detection. Quantification of the degradation spots was performed as previously described ⁸.

Electron microscopy. Cells were fixed with 2,5% glutaraldehyde in 0,1M cacodylate buffer and processed for EPON embedding and ultrathin sections as described ⁶². For cryoimmunolabeling, cells were fixed in a mixture of 2% paraformaldehyde and 0.125% glutaraldehyde in a 0.1M phosphate buffer pH7.4 during 48 hrs ⁶². Ultrathin sections were prepared with an ultracryomicrotome Leica EM UC7 and underwent single immunogold labeling with protein A conjugated to 10-nm diameter gold particles (Cell Microscopy Center, Department of Cell Biology, Utrecht University). Samples were analyzed with a Tecnai Spirit electron microscope (FEI Company, Eindhoven Netherlands) and digital acquisitions were made with a QUEMESA CCD camera (EMSIS GmbH, Münster, Germany).

Statistics and reproducibility. GraphPad Prism (GraphPad Software) was used for statistical analysis. Sample size was chosen based on estimates from pilot experiments and our published results such that appropriate statistical tests could yield significant results. Data were tested for normal distribution using the

D'Agostino-Pearson normality test and nonparametric tests were applied otherwise as indicated in the figure legends. Statistical significance was defined as *, $P < 0.05$; **, $P < 0.01$; ***, $P < 0.001$; ****, $P < 0.0001$; ns, not significant. Relationships between protein expression and distribution in tumors vs. normal adjacent tissues were estimated using Two tailed Student's t-test and Kruskal-Wallis test (for links between qualitative and quantitative parameters). Metastasis-free survival was determined as the interval between initial diagnosis and detection of the first metastasis. Survival distributions were estimated by the Kaplan–Meier method, and the significance of differences between survival rates were ascertained with the log-rank test. The Cox proportional hazards regression model was used to assess prognostic significance, and the results are presented as hazard ratio (HR) and 95% confidence interval (CI). The following variables were included in the analysis: SBR grade, lymph node status, macroscopic tumor size, PR status (all the classical variables with a P value under 0.10 in univariate analysis) and CORO1C or combined CORO1C and MT1-MMP mRNA expression. For animal studies, no animals were excluded from analyses and no blinding procedure was used.

See Supplementary Materials and Methods for additional cell lines, western blot analysis, patient cohort for mRNA analysis, RT-qPCR analysis, patient biopsies for western blot analysis, Immunohistochemistry analysis of human breast biopsies, Mammary fat pad and intraductal injections, Mammary imaging window surgical implantation and near-infrared multiphoton microscopy of mammary tumor xenografts.

References

1 Rowe RG, Weiss SJ. Breaching the basement membrane: who, when and how? Trends Cell Biol 2008; 18: 560-574.

2 Lodillinsky C, Infante E, Guichard A, Chaligne R, Fuhrmann L, Cyrta J et al. p63/MT1-MMP axis is required for in situ to invasive transition in basal-like breast cancer. Oncogene 2016; 35: 344-357.

3 Hotary K, Li XY, Allen E, Stevens SL, Weiss SJ. A cancer cell metalloprotease triad regulates the basement membrane transmigration program. Genes Dev 2006; 20: 2673-2686.

4 Wolf K, Wu YI, Liu Y, Geiger J, Tam E, Overall C et al. Multi-step pericellular proteolysis controls the transition from individual to collective cancer cell invasion. Nat Cell Biol 2007; 9: 893-904.

5 Linder S, Wiesner C, Himmel M. Degrading devices: invadosomes in proteolytic cell invasion. Annu Rev Cell Dev Biol 2011; 27: 185-211.

660 6 Artym VV, Zhang Y, Seillier-Moiseiwitsch F, Yamada KM, Mueller SC.
661 Dynamic interactions of cortactin and membrane type 1 matrix metalloproteinase at
662 invadopodia: defining the stages of invadopodia formation and function. *Cancer Res*
663 2006; 66: 3034-3043.

664

665 7 Steffen A, Le Dez G, Poincloux R, Recchi C, Nassoy P, Rottner K et al. MT1-
666 MMP-dependent invasion is regulated by TI-VAMP/VAMP7. *Curr Biol* 2008; 18: 926-
667 931.

668

669 8 Monteiro P, Rosse C, Castro-Castro A, Irondelle M, Lagoutte E, Paul-
670 Gilloteaux P et al. Endosomal WASH and exocyst complexes control exocytosis of
671 MT1-MMP at invadopodia. *J Cell Biol* 2013; 203: 1063-1079.

672

673 9 Gligorijevic B, Bergman A, Condeelis J. Multiparametric classification links
674 tumor microenvironments with tumor cell phenotype. *PLoS Biol* 2014; 12: e1001995.

675

676 10 Leong HS, Robertson AE, Stoletov K, Leith SJ, Chin CA, Chien AE et al.
677 Invadopodia are required for cancer cell extravasation and are a therapeutic target
678 for metastasis. *Cell Rep* 2014; 8: 1558-1570.

679

- 680 11 Yamaguchi H, Lorenz M, Kempiak S, Sarmiento C, Coniglio S, Symons M et
681 al. Molecular mechanisms of invadopodium formation: the role of the N-WASP-
682 Arp2/3 complex pathway and cofilin. *J Cell Biol* 2005; 168: 441-452.
- 683
- 684 12 Ayala I, Baldassarre M, Giacchetti G, Caldieri G, Tete S, Luini A et al. Multiple
685 regulatory inputs converge on cortactin to control invadopodia biogenesis and
686 extracellular matrix degradation. *J Cell Sci* 2008; 121: 369-378.
- 687
- 688 13 Weaver AM, Karginov AV, Kinley AW, Weed SA, Li Y, Parsons JT et al.
689 Cortactin promotes and stabilizes Arp2/3-induced actin filament network formation.
690 *Curr Biol* 2001; 11: 370-374.
- 691
- 692 14 Siton O, Ideses Y, Albeck S, Unger T, Bershadsky AD, Gov NS et al. Cortactin
693 releases the brakes in actin- based motility by enhancing WASP-VCA detachment
694 from Arp2/3 branches. *Curr Biol* 2011; 21: 2092-2097.
- 695
- 696 15 Cai L, Makhov AM, Schafer DA, Bear JE. Coronin 1B antagonizes cortactin
697 and remodels Arp2/3-containing actin branches in lamellipodia. *Cell* 2008; 134: 828-
698 842.
- 699

700 16 Chan KT, Creed SJ, Bear JE. Unraveling the enigma: progress towards
701 understanding the coronin family of actin regulators. Trends Cell Biol 2011; 21: 481-
702 488.

703

704 17 Abella JV, Galloni C, Pernier J, Barry DJ, Kjaer S, Carlier MF et al. Isoform
705 diversity in the Arp2/3 complex determines actin filament dynamics. Nat Cell Biol
706 2016; 18: 76-86.

707

708 18 Humphries CL, Balcer HI, D'Agostino JL, Winsor B, Drubin DG, Barnes G et
709 al. Direct regulation of Arp2/3 complex activity and function by the actin binding
710 protein coronin. J Cell Biol 2002; 159: 993-1004.

711

712 19 Foger N, Rangell L, Danilenko DM, Chan AC. Requirement for coronin 1 in T
713 lymphocyte trafficking and cellular homeostasis. Science 2006; 313: 839-842.

714

715 20 Clark ES, Weaver AM. A new role for cortactin in invadopodia: regulation of
716 protease secretion. Eur J Cell Biol 2008; 87: 581-590.

717

718 21 Clark ES, Brown B, Whigham AS, Kochaishvili A, Yarbrough WG, Weaver AM.
719 Aggressiveness of HNSCC tumors depends on expression levels of cortactin, a gene
720 in the 11q13 amplicon. Oncogene 2009; 28: 431-444.

721

722 22 Mader CC, Oser M, Magalhaes MA, Bravo-Cordero JJ, Condeelis J, Koleske
723 AJ et al. An EGFR-Src-Arg-cortactin pathway mediates functional maturation of
724 invadopodia and breast cancer cell invasion. *Cancer Res* 2011; 71: 1730-1741.

725

726 23 Rosse C, Lodillinsky C, Fuhrmann L, Nourieh M, Monteiro P, Irondelle M et al.
727 Control of MT1-MMP transport by atypical PKC during breast-cancer progression.
728 *Proc Natl Acad Sci U S A* 2014; 111: E1872-1879.

729

730 24 Molinie N, Gautreau A. The Arp2/3 Regulatory System and Its Deregulation in
731 Cancer. *Physiol Rev* 2018; 98: 215-238.

732

733 25 Wu L, Peng CW, Hou JX, Zhang YH, Chen C, Chen LD et al. Coronin-1C is a
734 novel biomarker for hepatocellular carcinoma invasive progression identified by
735 proteomics analysis and clinical validation. *J Exp Clin Cancer Res* 2010; 29: 17.

736

737 26 Ren G, Tian Q, An Y, Feng B, Lu Y, Liang J et al. Coronin 3 promotes gastric
738 cancer metastasis via the up-regulation of MMP-9 and cathepsin K. *Molecular cancer*
739 [electronic resource] 2012; 11: 67.

740

741 27 Liu C, Zhang S, Wang Q, Zhang X. Tumor suppressor miR-1 inhibits tumor
742 growth and metastasis by simultaneously targeting multiple genes. *Oncotarget* 2017;
743 8: 42043-42060.

744

745 28 Thal D, Xavier CP, Rosentreter A, Linder S, Friedrichs B, Waha A et al.
746 Expression of coronin-3 (coronin-1C) in diffuse gliomas is related to malignancy. *J*
747 *Pathol* 2008; 214: 415-424.

748

749 29 Ziemann A, Hess S, Bhuwania R, Linder S, Kloppenburg P, Noegel AA et al.
750 CRN2 enhances the invasiveness of glioblastoma cells. *Neuro Oncol* 2013; 15: 548-
751 561.

752

753 30 Hoshino D, Kirkbride KC, Costello K, Clark ES, Sinha S, Grega-Larson N et al.
754 Exosome secretion is enhanced by invadopodia and drives invasive behavior. *Cell*
755 *Rep* 2013; 5: 1159-1168.

756

757 31 Macpherson IR, Rainero E, Mitchell LE, van den Berghe PV, Speirs C,
758 Dozynkiewicz MA et al. CLIC3 controls recycling of late endosomal MT1-MMP and
759 dictates invasion and metastasis in breast cancer. *J Cell Sci* 2014; 127: 3893-3901.

760

761 32 Marchesin V, Castro-Castro A, Lodillinsky C, Castagnino A, Cyrta J, Bonsang-
762 Kitzis H et al. ARF6-JIP3/4 regulate endosomal tubules for MT1-MMP exocytosis in
763 cancer invasion. J Cell Biol 2015; 211: 339-358.

764

765 33 Castro-Castro A, Marchesin V, Monteiro P, Lodillinsky C, Rosse C, Chavrier P.
766 Cellular and Molecular Mechanisms of MT1-MMP-Dependent Cancer Cell Invasion.
767 Annu Rev Cell Dev Biol 2016; 32: 555-576.

768

769 34 Gomez TS, Billadeau DD. A FAM21-containing WASH complex regulates
770 retromer-dependent sorting. Dev Cell 2009; 17: 699-711.

771

772 35 Derivery E, Sousa C, Gautier JJ, Lombard B, Loew D, Gautreau A. The Arp2/3
773 activator WASH controls the fission of endosomes through a large multiprotein
774 complex. Dev Cell 2009; 17: 712-723.

775

776 36 Holtta-Vuori M, Vainio S, Kauppi M, Van Eck M, Jokitalo E, Ikonen E.
777 Endosomal actin remodeling by coronin-1A controls lipoprotein uptake and
778 degradation in macrophages. Circ Res 2012; 110: 450-455.

779

780 37 Kirkbride KC, Hong NH, French CL, Clark ES, Jerome WG, Weaver AM.
781 Regulation of late endosomal/lysosomal maturation and trafficking by cortactin
782 affects Golgi morphology. Cytoskeleton (Hoboken) 2012; 69: 625-643.

783

784 38 Sinha S, Hoshino D, Hong NH, Kirkbride KC, Grega-Larson NE, Seiki M et al.
785 Cortactin promotes exosome secretion by controlling branched actin dynamics. J Cell
786 Biol 2016; 214: 197-213.

787

788 39 Smith SE, Mellor P, Ward AK, Kendall S, McDonald M, Vizeacoumar FS et al.
789 Molecular characterization of breast cancer cell lines through multiple omic
790 approaches. Breast Cancer Res 2017; 19: 65.

791

792 40 Juin A, Billottet C, Moreau V, Destaing O, Albiges-Rizo C, Rosenbaum J et al.
793 Physiological type I collagen organization induces the formation of a novel class of
794 linear invadosomes. Molecular biology of the cell 2012; 23: 297-309.

795

796 41 Chan KT, Roadcap DW, Holoweckyj N, Bear JE. Coronin 1C harbours a
797 second actin-binding site that confers co-operative binding to F-actin. Biochem J
798 2012; 444: 89-96.

799

800 42 Cai L, Makhov AM, Bear JE. F-actin binding is essential for coronin 1B
801 function in vivo. J Cell Sci 2007; 120: 1779-1790.

802

803 43 Behbod F, Kittrell FS, LaMarca H, Edwards D, Kerbawy S, Heestand JC et al.
804 An intraductal human-in-mouse transplantation model mimics the subtypes of ductal
805 carcinoma in situ. *Breast Cancer Res* 2009; 11: R66.

806

807 44 Mukherjee S, Maxfield FR. Lipid and cholesterol trafficking in NPC. *Biochim*
808 *Biophys Acta* 2004; 1685: 28-37.

809

810 45 Liscum L, Faust JR. The intracellular transport of low density lipoprotein-
811 derived cholesterol is inhibited in Chinese hamster ovary cells cultured with 3-beta-
812 [2-(diethylamino)ethoxy]androst-5-en-17-one. *J Biol Chem* 1989; 264: 11796-11806.

813

814 46 Wang J, Tsouko E, Jonsson P, Bergh J, Hartman J, Aydogdu E et al. miR-206
815 inhibits cell migration through direct targeting of the actin-binding protein coronin 1C
816 in triple-negative breast cancer. *Mol Oncol* 2014; 8: 1690-1702.

817

818 47 McGowan PM, Duffy MJ. Matrix metalloproteinase expression and outcome in
819 patients with breast cancer: analysis of a published database. *Ann Oncol* 2008; 19:
820 1566-1572.

821

822 48 Perentes JY, Kirkpatrick ND, Nagano S, Smith EY, Shaver CM, Sgroi D et al.
823 Cancer cell-associated MT1-MMP promotes blood vessel invasion and distant
824 metastasis in triple-negative mammary tumors. *Cancer Res* 2011; 71: 4527-4538.

825

826 49 Rosentreter A, Hofmann A, Xavier CP, Stumpf M, Noegel AA, Clemen CS.
827 Coronin 3 involvement in F-actin-dependent processes at the cell cortex. *Exp Cell*
828 *Res* 2007; 313: 878-895.

829

830 50 Yu X, Zech T, McDonald L, Gonzalez EG, Li A, Macpherson I et al. N-WASP
831 coordinates the delivery and F-actin-mediated capture of MT1-MMP at invasive
832 pseudopods. *J Cell Biol* 2012; 199: 527-544.

833

834 51 Cai L, Marshall TW, Uetrecht AC, Schafer DA, Bear JE. Coronin 1B
835 coordinates Arp2/3 complex and cofilin activities at the leading edge. *Cell* 2007; 128:
836 915-929.

837

838 52 Eckert MA, Lwin TM, Chang AT, Kim J, Danis E, Ohno-Machado L et al.
839 Twist1-induced invadopodia formation promotes tumor metastasis. *Cancer Cell* 2011;
840 19: 372-386.

841

842 53 Puthenveedu MA, Lauffer B, Temkin P, Vistein R, Carlton P, Thorn K et al.
843 Sequence-dependent sorting of recycling proteins by actin-stabilized endosomal
844 microdomains. *Cell* 2010; 143: 761-773.

845

846 54 Gomez TS, Gorman JA, de Narvajas AA, Koenig AO, Billadeau DD.
847 Trafficking defects in WASH-knockout fibroblasts originate from collapsed endosomal
848 and lysosomal networks. Mol Biol Cell 2012; 23: 3215-3228.

849

850 55 Hong NH, Qi A, Weaver AM. PI(3,5)P2 controls endosomal branched actin
851 dynamics by regulating cortactin-actin interactions. J Cell Biol 2015; 210: 753-769.

852

853 56 Willett R, Martina JA, Zewe JP, Wills R, Hammond GRV, Puertollano R. TFEB
854 regulates lysosomal positioning by modulating TMEM55B expression and JIP4
855 recruitment to lysosomes. Nat Commun 2017; 8: 1580.

856

857 57 Sakurai-Yageta M, Recchi C, Le Dez G, Sibarita JB, Daviet L, Camonis J et al.
858 The interaction of IQGAP1 with the exocyst complex is required for tumor cell
859 invasion downstream of Cdc42 and RhoA. J Cell Biol 2008; 181: 985-998.

860

861 58 Marchesin V, Montagnac G, Chavrier P. ARF6 promotes the formation of Rac1
862 and WAVE-dependent ventral F-actin rosettes in breast cancer cells in response to
863 epidermal growth factor. PLoS One 2015; 10: e0121747.

864

865 59 Sibarita JB. Deconvolution microscopy. Advances in biochemical
866 engineering/biotechnology 2005; 95: 201-243.

867

868 60 Lamprecht MR, Sabatini DM, Carpenter AE. CellProfiler: free, versatile
869 software for automated biological image analysis. *BioTechniques* 2007; 42: 71-75.

870

871 61 Castro-Castro A, Janke C, Montagnac G, Paul-Gilloteaux P, Chavrier P.
872 ATAT1/MEC-17 acetyltransferase and HDAC6 deacetylase control a balance of
873 acetylation of alpha-tubulin and cortactin and regulate MT1-MMP trafficking and
874 breast tumor cell invasion. *Eur J Cell Biol* 2012; 91: 950-960.

875

876 62 Hurbain I, Romao M, Bergam P, Heiligenstein X, Raposo G. Analyzing
877 Lysosome-Related Organelles by Electron Microscopy. *Methods Mol Biol* 2017;
878 1594: 43-71.

879

880

881

882

Acknowledgments. The authors greatly acknowledge the Breast Cancer Study Group and patients of Institut Curie for breast tumor samples. They thank the Cell and Tissue Imaging facility (PICT-IBiSA) and Nikon Imaging Centre, Institut Curie, member of the French National Research Infrastructure France-BioImaging (ANR10-INBS-04) for help with image acquisition and Dr Jakko van Rheenen for help with the mammary window and intravital imaging. A.C. was supported by a grant from Worldwide Cancer Research (Grant 16-1235 to P.C.), A.C.C. by an EMBO Long Term postdoctoral fellowship and a grant from '*Institut National du Cancer*' (INCA_6521 to P.C.), A.G. by INVADE grant from ITMO Cancer (Call Systems Biology 2012) to P.C., S.A.G. by a grant from INCa (INCa 2014-11/474/AB-SD to P.C.) and A.A.N. and C.S.C by a grant from the German Research Foundation (DFG NO 113/22-2). The intravital imaging was supported by the Fondation pour la Recherche Médicale (FRM N° DGE20111123020), the Canceropole-IdF (n°2012-2-EML-04-IC-1), InCA (Cancer National Institute, n° 2011-1-LABEL-IC-4) and SiRIC (INCa-DGOS- 4654). This work was supported by grants from '*Institut National du Cancer*' (INCa 2014-11/474/AB-SD and INCA_6521), Worldwide Cancer Research (Grant 16-1235) and '*Equipe labellisée 2015*' from '*Ligue Nationale contre le Cancer*' to P.C.

Author contributions

AC carried out invadopodia formation and collagen degradation assays with the help of AZM and characterized the effects of CORO1C depletion on endolysosomal morphology and position. ACC who initiated the study, generated the cell lines stably expressing ^{GFP}CORO1C constructs and analyzed CORO1B and -1C expression in lysates of breast cancer cell lines provided by TD. LF and AVS generated the breast cancer TMA, performed CORO1C IHC labeling and scored the breast tumor TMA for CORO1C expression with the help of CEK. SV and IB generated the invasive breast cancer cohort and performed RT-qPCR and multivariate analyses. MI performed multicellular spheroid invasion assays, analyzed the phenotype of cells silenced for cortactin and performed intravital imaging. AG, CL and SAG carried out mammary gland injections and analyzed tumor xenografts. MR and GR performed electron microscopy analyses. JEB, AAN and CSC provided essential reagents. PC supervised the study and wrote the manuscript with contribution of all authors.

Figure Legends

Figure 1. Patients displaying high CORO1C and MT1-MMP mRNA expression

have poor outcomes in breast cancer. (A) Whole-cell lysates from human breast carcinoma cell lines and Jurkat T cells were normalized for protein concentration and immunoblotted with indicated antibodies. Stratification of breast cancer cell lines in Normal-like, TNBC, Luminal and HER2 subtypes was according to ³⁹. **(B-E)** Expression of the indicated proteins in the different cell lines divided in four subtypes was normalized to GAPDH level. Protein levels were analyzed in 2 to 3 experiments for each protein in each cell line and plots correspond to average expression levels \pm SEM in each subtype. **(F)** Expression of the indicated genes was analyzed by RT-qPCR in 446 mRNA tumor samples. Patients exhibiting high CORO1C mRNA have reduced MFS (log-rank test using optimal cutoff of 1.52; $p=0.00082$). Number of patients in each subgroup is indicated in parenthesis. **(G)** Correlation between indicated gene transcripts was analyzed using the Spearman's rank correlation test (in bold type). *P* values are in italics. **(H)** Patients exhibiting both high CORO1C and MT1-MMP mRNAs have reduced MFS (log-rank test using optimal cut-off of 1.52 for CORO1C and 1.30 for MT1-MMP; $P=0.00048$).

Figure 2. Increased CORO1C expression in invasive breast cancers. (A, B)

CORO1C immunohistochemistry staining on sections of human invasive breast cancer (IBC) tissue microarray showing adjacent non-neoplastic tissue (Normal) and representative TNBC and HER2+ breast cancers. **(C, D)** Semi-quantitative analysis of CORO1C protein expression by the H-score method comparing adjacent breast epithelial tissues and carcinoma tissues (C) or in the different subtypes (D). Two tailed t-test (C); Kruskal-Wallis test (D).

Figure 3. CORO1C is required for 3D invasion and invadopodia function. (A)

MDA-MB-231 cells expressing ^{GFP}CORO1C (green) were embedded in 2.2 mg/ml fluorescent type I collagen (magenta) and polymerization was induced at neutral pH at 37°C. Cells were fixed after 12-16 h and stained for cortactin (red). The nucleus is stained with DAPI (blue). The image is a single optical plane from a z-stack (Supplementary Movie S1). The low magnification inset is a projection of the z-stack of images (collagen is omitted). Inset 1 shows separated channels corresponding to the boxed region. **(B)** Cells in 3D collagen (magenta) stained for cleaved collagen neoepitope (Col1-³⁴C antibody, yellow) and F-actin (blue). DAPI-stained nuclei are shown in cyan. **(C)** MDA-MB-231 cells expressing ^{GFP}CORO1C (green) were incubated on a thick layer of fibrous type I collagen (magenta). Curvilinear invadopodia forming in association with collagen fibrils (cyan) were labeled for TKS5 (red). Insets show separated channels corresponding to the boxed region. **(D)** Phalloidin-labeled multicellular spheroids of MDA-MB-231 cells expressing GFP or ^{GFP}CORO1C after 2 days in 3D collagen I (T2). Insets show spheroids immediately after embedding in collagen (T0). **(E)** Mean invasion area of multicellular spheroids at T2 in the presence or absence of GM6001 normalized to mean spheroid area at T0 ± SEM. *n*, spheroid number. Two-way ANOVA. **(F)** Quantification of invadopodia-associated TKS5 signal in MDA-MB-231 cells expressing GFP, ^{GFP}CORO1C or mutant ^{GFP}CORO1C_{R28D/2KE} plated on a thick layer of type I collagen as in panel C. Y-axis indicates TKS5 area normalized to total cell area and to mean value in MDA-MB-231 cells (as percentage) ± SEM. *n*, number of cells analyzed from three independent experiments. Kruskal-Wallis test. **(G)** TKS5-positive invadopodia in MDA-MB-231 cells knocked down for CORO1C, CORO1B or both as in panel F. *n*, number of cells analyzed from five (siNT), three (siCORO1C^{#04} and ^{#08}) or two

(siCORO1B and siCORO1B+C^{#04}) independent experiments. **(H)** MDA-MB-231 cells expressing CORO1B^{GFP} (green) and MT1-MMP^{mCh} (red) plated on fibrous type I collagen (magenta). CORO1B and MT1-MMP colocalize in invadopodia forming in association with the collagen fibers (inset 1). CORO1B-positive puncta are also visible on MT1-MMP endolysosomes (inset 2). **(I)** Representative images of pericellular collagenolysis detected with Col1-^{3/4}C antibody (black signal in the inverted images). Nuclei were stained with DAPI (red). **(J, K)** Collagen degradation measured by Col1-^{3/4}C neoepitope staining by indicated cell populations normalized to GFP-expressing (I) or siNT-treated (J) control cells \pm SEM; *n*, number of cells analyzed from three independent experiments. Data were transformed using the log transformation $y=\log(y)$ to make data conform to normality and analyzed using one-way ANOVA.

Figure 4. In vivo association of CORO1C-positive invadopodia with ECM fibers.

(A-D) Near-infrared multiphoton microscopy images of tumor sections of 8-week-old fat pad tumor xenografts from MDA-MB-231/^{GFP}CORO1C (panels A to C) or MDA-MB-231/^{GFP}CORO1C_{R28D/2KE} cells (panel D). Collagen fibers detected by second harmonic generation (SHG, magenta). **(G-I)** Time-course of the growth and invasion of MCF10DCIS.com/^{GFP}CORO1C intraductal tumor xenograft monitored by near-infrared multiphoton microscopy 5 to 7-week post injection. All images are single optical sections from z-stack except in panel G and H, which show maximum intensity projections of indicated optical planes. Insets are higher magnification of boxed regions. White arrows point to accumulations of ^{GFP}CORO1C in association with collagen fibers.

Figure 5. Altered MT1-MMP endosome positioning and morphology upon CORO1C knockdown. (A) Still image from live cell confocal microscopy sequence

of MDA-MB-231 cells expressing MT1-MMP^{mCh} and ^{GFP}CORO1C (see Supplementary Movie S2). Inset is a high magnification of the boxed region. Bottom row shows the fluorescence intensity profiles of MT1-MMP^{mCh} and ^{GFP}CORO1C along the dotted line. **(B)** High magnification of MDA-MB-231 cell expressing MT1-MMP^{mCh} and ^{GFP}CORO1C_{R28D/2KE} as in panel A. Fluorescence intensity profiles are shown. **(C)** MDA-MB-231 cells expressing MT1-MMP^{mCh} (red) and ^{GFP}CORO1C (green) stained for CTTN (blue). **(D)** Cryoimmunoelectron microscopy of MDA-MB-231 cells expressing ^{GFP}CORO1C. The micrograph shows the localization of ^{GFP}CORO1C on LE/lysosomes (asterisk) visualized with anti-GFP antibodies and secondary antibodies coupled to 10-nm diameter protein A-gold (arrows). Arrowheads point to ^{GFP}CORO1C associated with the cytosolic face of the plasma membrane. **(E-H)**. Confocal fluorescence microscopy images of MDA-MB-231 cells expressing MT1-MMP^{mCh} (red) superimposed with the phase-contrast image (grey). Cells are treated with indicated siRNAs. Cell contour is shown with dashed line. **(I)** Distribution of MT1-MMP^{mCh}-positive endosomes in MDA-MB-231 cells treated with indicated siRNAs. Mean percentage of MT1-MMP-positive endosomes according to their cell center-to-cell periphery position \pm SEM from three independent experiments. **(J)** Proportion of MDA-MB-231 cells (%) with juxtanuclear clustered or scattered MT1-MMP^{mCh} endosome distribution from four to five independent experiments (Fig. S6C-E).

Figure 6. Knockdown of CORO1C affects the distribution of MT1-MMP-positive endolysosomes and JIP4 and CTTN association. **(A-C)** Indirect immunofluorescence analysis of MDA-MB-231 cells expressing MT1-MMP^{mCh} treated with indicated siRNAs with CTTN (blue) and JIP4 (green) antibodies. DAPI-stained nuclei are shown in cyan. **(D, E)** CTTN (D) and JIP4 (E) association with the cytosolic

1016 face of MT1-MMPmCh-positive endosomes analyzed based on images such as in
1017 panel A-C, compared with siNT-treated cells \pm SEM from three independent
1018 experiments. n, number of cells analyzed for each population. **(F-I)** Electron
1019 microscopy of ultrathin sections of epon-embedded cells treated with indicated
1020 siRNAs. Notice the large aggregated endolysosomes in CORO1C-depleted cells
1021 (asterisks). N, nucleus; LE, endolysosome; m, mitochondria.

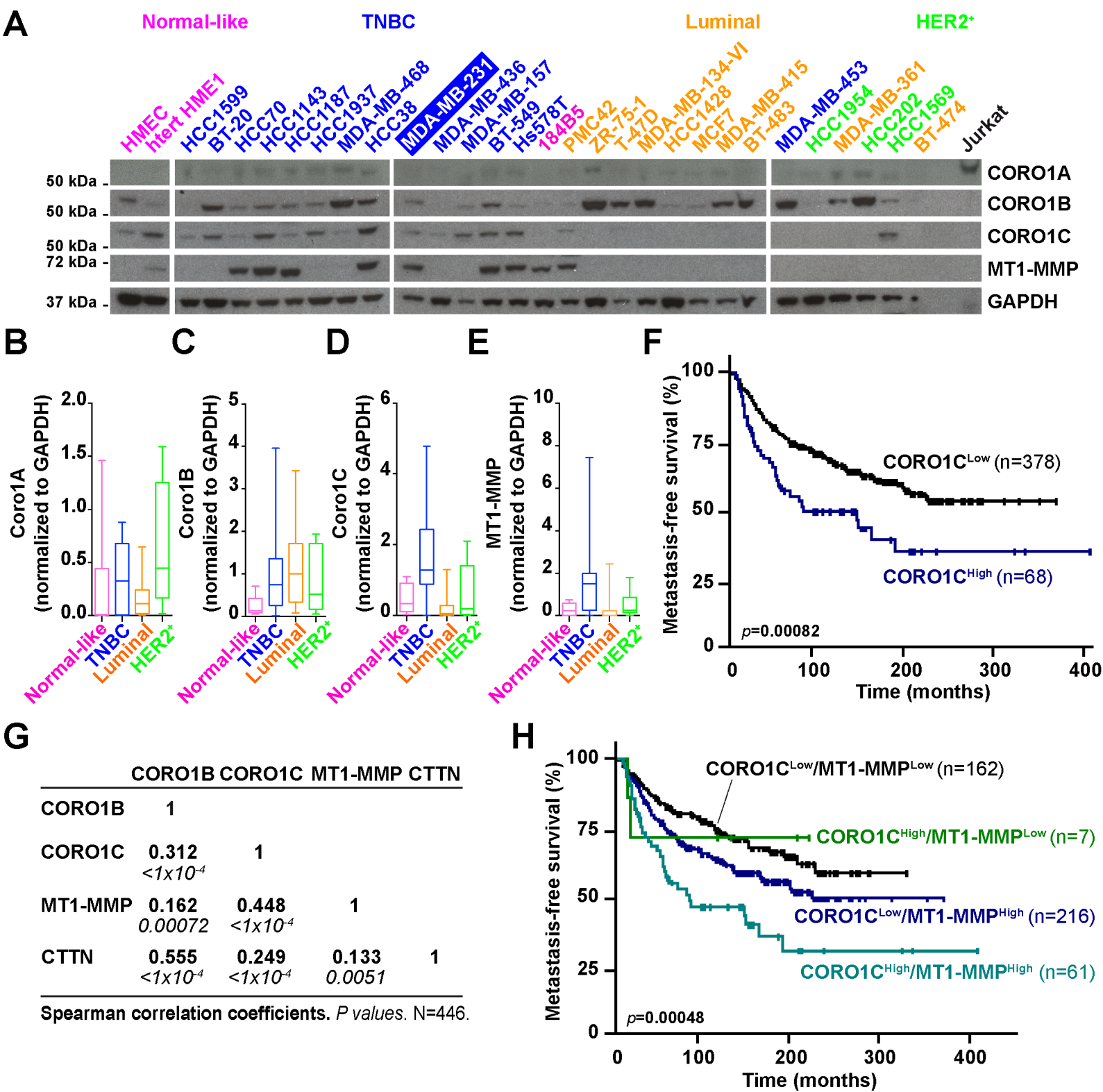


FIGURE 1

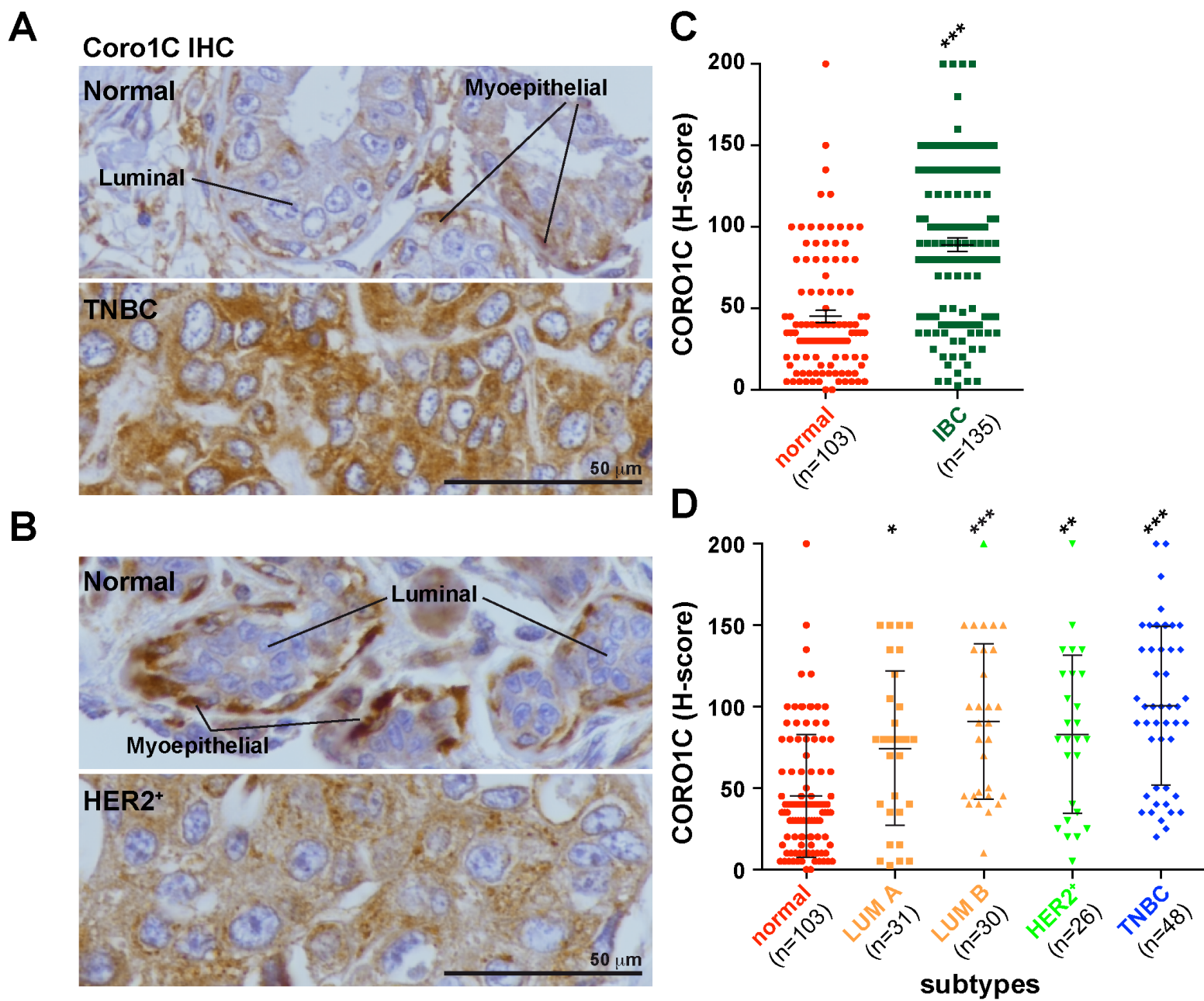


FIGURE 2

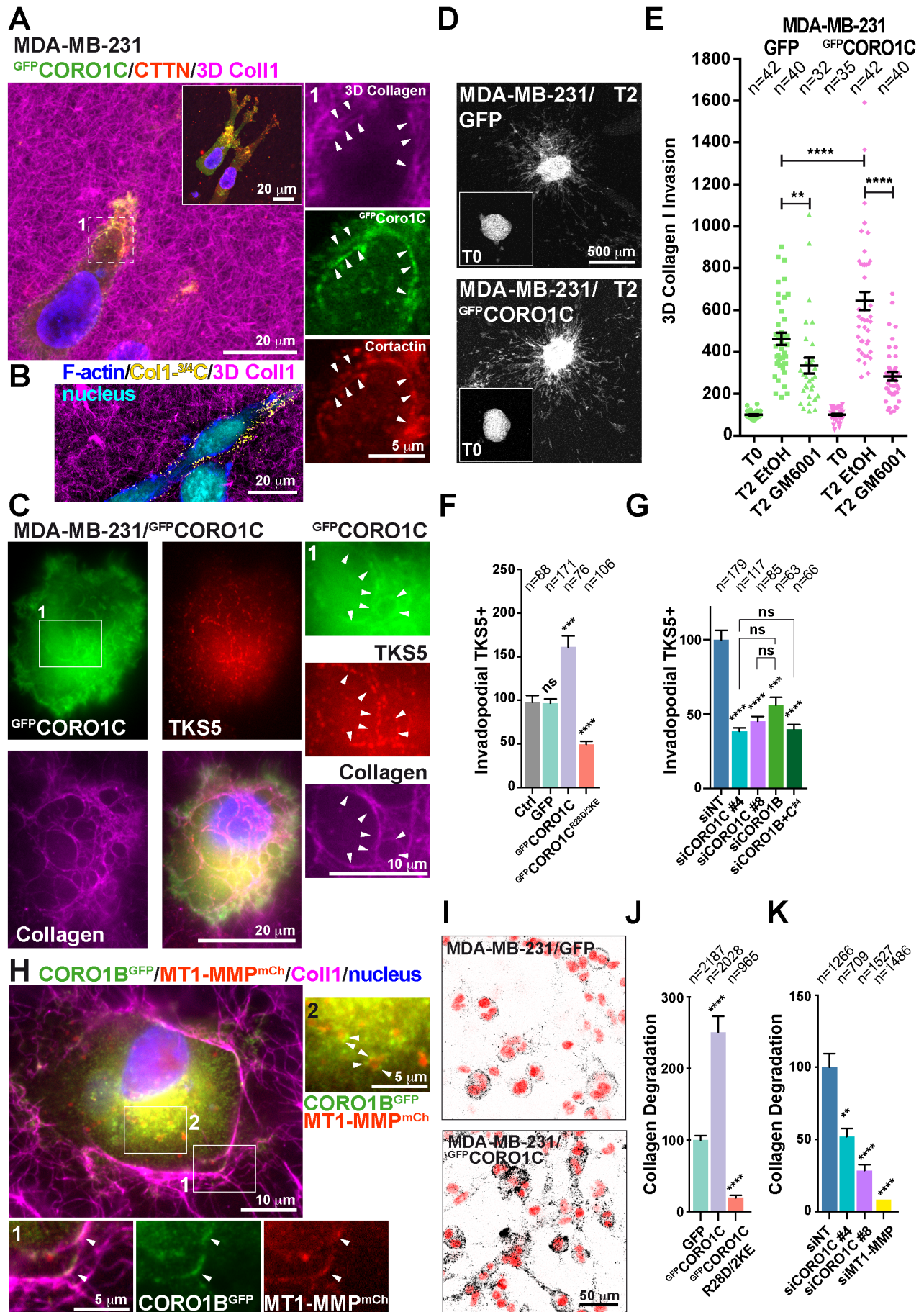
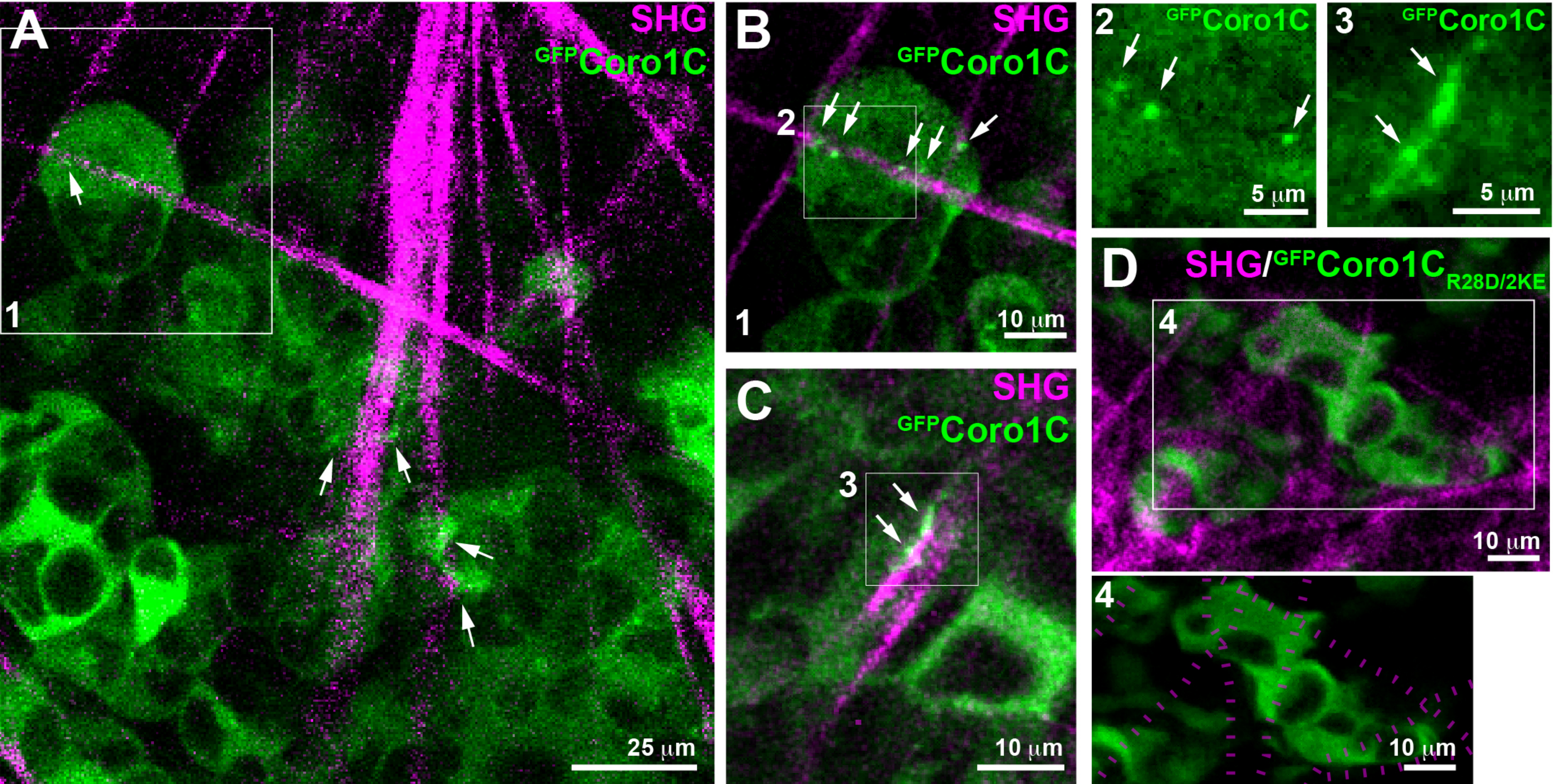


FIGURE 3

Fat pad injection - MDA-MB-231/^{GFP}Coro1C (8-week pi)



Intraductal injection - MCF10DCIS.com/^{GFP}Coro1C

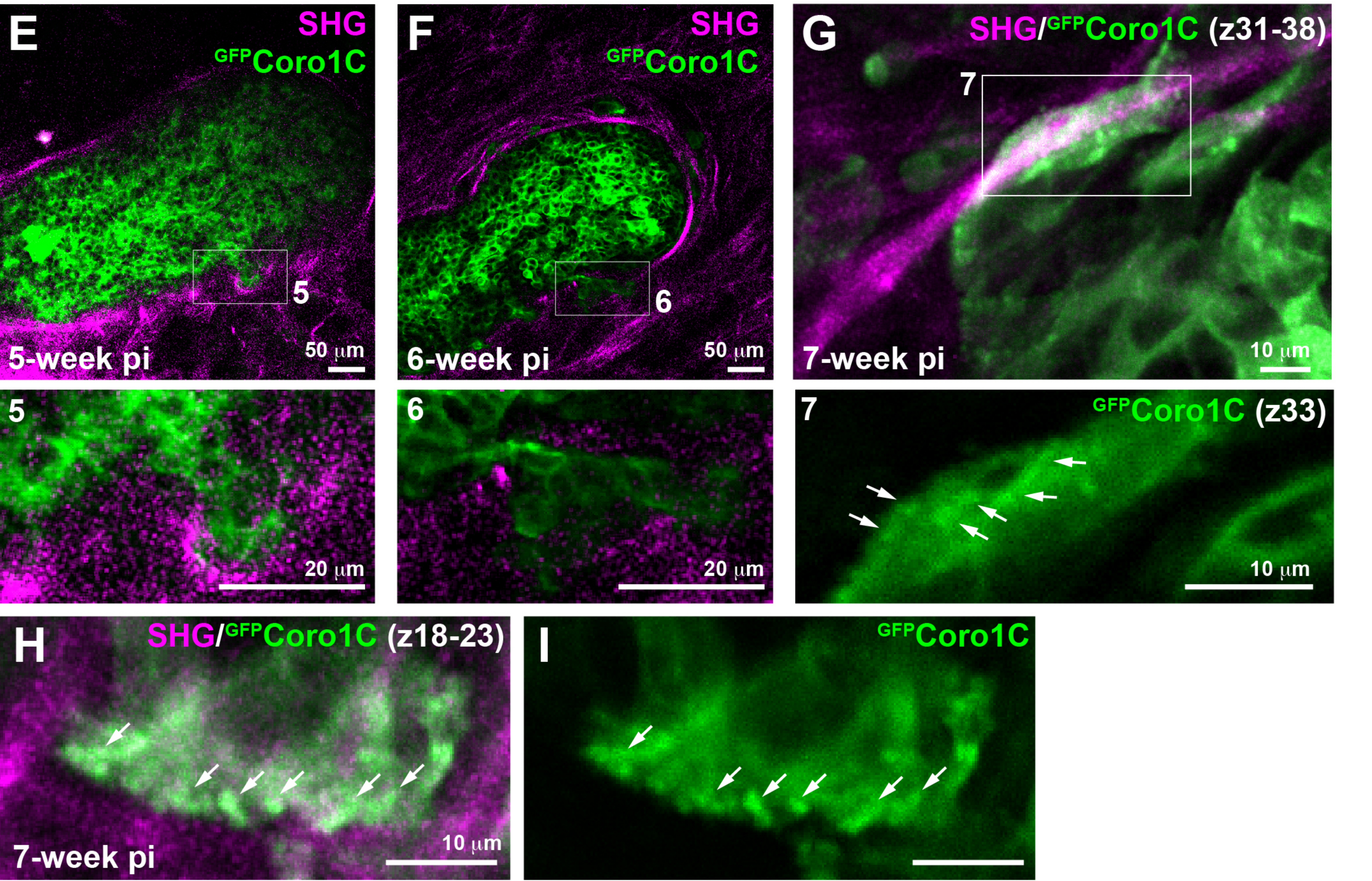


FIGURE 4

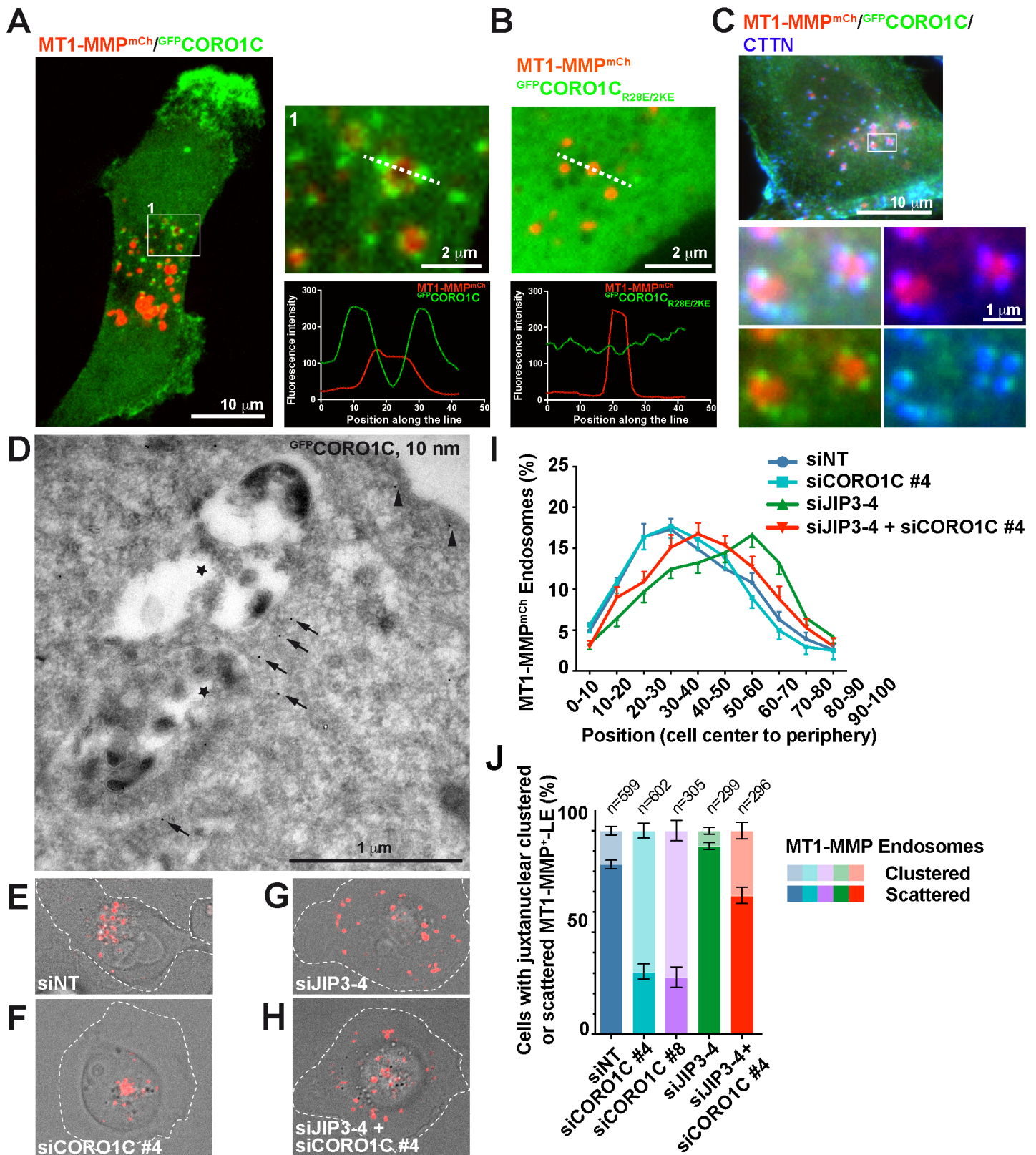


FIGURE 5

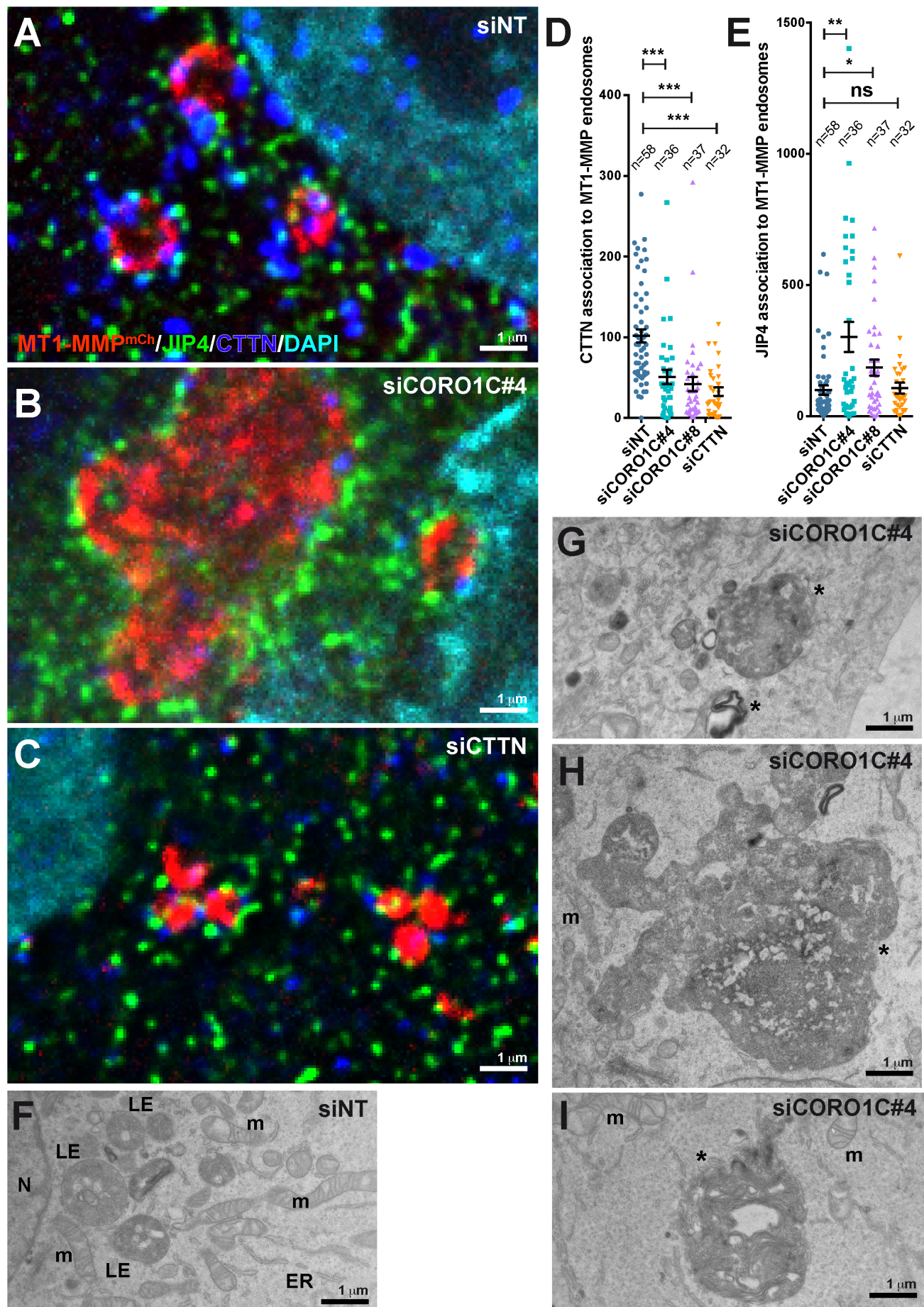


FIGURE 6